Congresso de Métodos Numéricos em Engenharia 2015
Lisboa, 29 de Junho a 2 de Julho 2015

NUMERICAL SIMULATION OF LIQUID SEMI–CRYSTALLINE PLANAR FILM CASTING PROCESSES

J. I. Ramos

Escuela de Ingenierías
Universidad de Málaga
Dr. Ortiz Ramos, s/n, 29071 Málaga, Spain
e-mail: jirs@lcc.uma.es

Keywords: Film casting, polymers, crystallization, molecular orientation, finite differences

Abstract. *A two-dimensional model of the film casting process of incompressible semi-crystalline polymers that accounts for the molecular orientation and the crystallization of the polymer macromolecules and the heat exchanges with the surrounding gases is presented. The polymer's rheology is assumed to consist of Newtonian and polymeric contributions that depend on the temperature, molecular orientation and crystallization. The molecular orientation model is based on the Doi-Edwards probability density function model, uses a moment expansion and results in a symmetric orientation tensor, whereas the crystallization model is based on Ziabicki's approximation and depends on the velocity and degree of molecular orientation. A compressible boundary layer approximation is used to determine the velocity and temperature fields of the gases that surround the planar film. The unknown curvilinear geometries of the film and the boundary layer for the gases that surround the film were mapped into unit squares, and the governing equations were written in strong-conservation law in their respective (mapped) domains where they were discretized by means of second-order accurate finite difference formulae because of the low Reynolds numbers that characterize planar film casting and solved iteratively using a pseudo-time formulation until specified convergence criteria were satisfied. The grid spacing was not uniform and grid points were concentrated in regions where large gradients occurred. The numerical results show that the polymer's molecular orientation depends mainly on the film's strain rate which increases sharply near the die's exit if the heat exchanges with the surrounding gases are large, or near the take-up drum if heat exchanges are small. It has also been found that an increase in the molecular orientation results in an increase of both the degree of crystallization and the effective dynamic viscosity of the polymeric planar film.*

1 INTRODUCTION

Planar film casting is a manufacturing process that has been used to produce polymer films that have applications in food packaging, coating, etc. [1]. In planar casting, synthetic films are produced by extruding a molten polymer [2]. The extruded film is stretched in air for a short distance and cooled on a chill roll; the collected film may then be subjected to, for example, biaxial orientation or coating on a substrate [3]. A schematic cross–section of a single–layer film casting process is shown in Figure 1, where x and y denote the longitudinal and transverse coordinates, respectively; the z coordinate not shown in the figure is the spanwise or film's width direction, and the velocity components along x, y and z directions are u, v ad w, respectively.
The flow between the die and the chill roll may be assumed to be elongational if the film's slenderness ratio, i.e., the ratio of the film's thickness at the die's exit to the film's length, and the film's thickness–to–width ratio are much smaller than one. Except for guided films, the film's width decreases along the longitudinal or drawing direction as a result of surface tension, die swell and edge stresses [4] that lead to the formation of edge beads that bound a central area whose thickness is almost independent of the spanwise direction [5]. Trimming of the edge beads is carried out before the film is used in industrial applications.

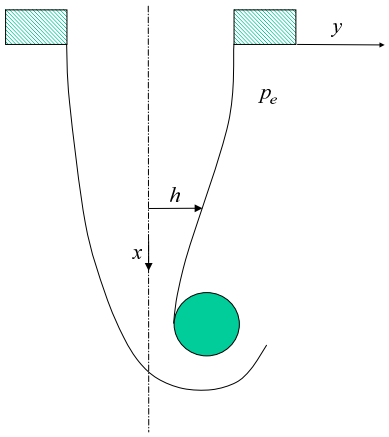

Figure 1: Schematic of a single–layer film casting process.

Most of the analytical and numerical studies of planar film casting processes performed to–date have been carried out by means of 1– or 1.5–dimensional, i.e., 1D and 1.5D, respectively, models, and have been mainly concerned with different rheologies under isothermal conditions, and stability. In 1D models, the film's width is assumed to be infinite so that there are no spanwise variations and, therefore, these models cannot

deal with the film's neck–in and edge bead formation. In addition, these models assume that the film's is slender, the molten polymer's longitudinal velocity and pressure are only functions of the coordinate along the drawing direction, and have been derived by applying the mean–value theorem of integration to the integral form of the linear momentum and continuity equations. They can also be derived by means of either Taylor's series expansions in the transverse coordinate or asymptotic methods for small slenderness ratios and small Reynolds numbers.

In 1.5D models, the film's lateral neck–in is accounted for by using a similar approach for the longitudinal velocity component and the pressure as that of 1D models, and the transverse and spanwise velocity components are assumed to depend linearly on the transverse coordinate so that the film's thickness is a function of both the longitudinal and spanwise coordinates and, therefore, the kinematic condition at the film's lateral edges may be applied. The assumption that the transverse and spanwise velocity components are linear functions of the transverse coordinate made in 1.5D models can only be justified if the film's is slender and the film's thickness–to–width ratio is much smaller than unity. Moreover, although 1.5D models account for the kinematic conditions at the film's edges and, therefore, for the film's neck–in, they cannot deal with the dynamic and thermal conditions there; the former are responsible for the edge bead formation.

One-dimensional models of planar film casting that account for the heat exchanges between the film and its surroundings include the 1D continuum mechanics–based model of Barot and Rao [6] who considered the amorphous and crystalline phases with viscoelastic Maxwell–type and neo–Hookean rheologies, respectively, and employed a thermodynamic criterion for the onset of crystallization which is based on the maximization of the rate of dissipation, but they did not consider the molecular orientation. A 1D model was also developed by Beaulne and Mitsoulis [7] who employed an integral constitutive equation to account for the rheology of the polymer melt, but they did not account for the polymer's molecular orientation and crystallization.

The 1.5D model developed by Lamberti et al. [8, 9] uses a Newtonian rheology for the molten polymer whose dynamic viscosity depends in an Arrhenius manner on both the temperature and the degree of crystallization; the latter was modelled by means of the isokinetic model proposed by Nakamura [10]. Barq et al. [11] developed a 1.5D model which does not consider molecular orientation and crystallization. Shiromoto [12] analyzed the neck-in phenomenon in film casting processes by means of a 1.5D model that employs the Phan-Thien/Tanner rheology and showed that neck-in is determined by the ratio of the planar to the elongational viscosity rather than by the strain hardening associated with the uniaxial elongational viscosity. A 1.5D model and a Giesekus rheology have been used by Zavinska et al. [13] in their studies of draw resonance of non-isothermal film casting of polymers; these authors, as well as many others, did not account for heat diffusion in the stretching direction, although they included a heat exchange term in their one-dimensional energy equation.

Some examples of two-dimensional models of film casting processes include that of Silagy

et al. [14] who employed a finite element method in their studies of isothermal film casting in the (x, z)–plane and assumed that the transverse velocity component was a linear function of the transverse coordinate; therefore, these authors accounted for the film's neck–in. A similar approach was proposed by Anturkar and Co [15] and Christodoulou et al. [16] who also made use of a membrane approximation to determine the film's thickness as a function of the longitudinal and spanwise coordinates, but constrained the film's edges to prevent neck–in. A similar model was proposed by Sakaki et al. [17] who claimed to have developed a 3D formulation based on the neglect of inertia and volumetric forces in the linear momentum equation; however, the film's edges were assumed to be flat.
Non–isothermal film casting processes have been considered by Kim et al. [18] and Shin et al. [19]; these authors used the upper convective Maxwell and Phan-Thien/Tanner rheological models, respectively, and assumed that the film's edges are flat. In addition, their energy equation contains no diffusion terms, although it contains a Newton's cooling term for the heat exchanges between the film and its surroundings. Similar models have been proposed by Sollogoub et al. [20] and Satoh et al. [21] who employed an upper convective Maxwell rheology and Newtonian and Larson's rheologies, respectively, and an energy equation analogous to that of Kim et al. [18] and Shin et al. [19].
Two-dimensional models of the film casting of semi-crystalline compressible polymers have been developed by the author [22]; these models assume that the film's width is infinite so that the flow is two–dimensional in the (x, y)– plane, account for the dependence of the molten polymer's density on pressure and temperature, and include a mixed Newtonian-polymeric rheology and models for the molecular orientation and crystallization. For incompressible, liquid semi-crystalline, slender polymer films and fibers at low Reynolds and Biot numbers, these two–dimensional models reduce to the one–dimensional equations for the film's thickness or fiber's radius, temperature, axial velocity, degree of crystallization and molecular orientation tensor deduced by the author by means of a long–wave asymptotic expansion [23, 24, 25].
In this paper, a two-dimensional model for the casting of incompressible, liquid semi-crystalline films is proposed. The model is based on that developed by the author [22] for compressible polymers, accounts for longitudinal and transverse heat diffusion and uses Ziabicki's model [26] for the crystallization, either accounts for the gas boundary layer on the film's surface or employs heat transfer correlations that account for forced and natural convection and radiation at the film's outer surface, and considers three–layer films that are of current interest for food packaging and protection, coating and materials applications.
The paper has been arranged as follows. In the next section, a brief discussion of the mass, linear momentum and energy conservation equations, and for the molecular orientation order parameter and the degree of crystallization is presented. This section is followed by a description of the two numerical methods that have been used to solve the governing equations, the presentation of some sample results and some conclusions.

2 PROBLEM FORMULATION

We consider a three–layer planar film consisting of an inner layer or core, $-h(x)/2 \leq y \leq h(x)/2$, of thickness $h(x)$, surrounded by two identical outer layers or cladding, $-H(x) - h(x)/2 \leq y \leq -h(x)/2$ and $h(x)/2 \leq z \leq h(x)/2 + H(x)$ of thickness $H(x)$ that surround the inner one. The film width is assumed to be infinite so that the flow is two-dimensional in the $x - y$ plane, and identical polymers and processing conditions are used in the two cladding layers, so that the problem is symmetric with respect to the x–axis.

The molten polymers exiting from the planar die are assumed to be incompressible, homogeneous, two-phase flows of constant density, i.e., the amorphous and crystalline phases have the same velocity, temperature and density. Under these conditions, the governing equations for each polymer layer may be written as

$$\nabla \cdot \mathbf{v} = 0, \tag{1}$$

$$\rho \mathbf{v} \cdot \nabla \mathbf{v} = -\nabla p + \rho \mathbf{g} + \nabla \cdot \sigma, \tag{2}$$

$$\rho C_p \mathbf{v} \cdot \nabla T = \nabla \cdot (K \nabla T) + \rho L_c \dot{\theta}, \tag{3}$$

where viscous dissipation has been neglected, ρ is the (constant) density, $\mathbf{v} = (u, v)^T$ is the two-dimensional velocity vector whose components along and across the film are u and v, respectively, the superscript T denotes transpose, p and T are the pressure and temperature, respectively, C_p and K are the polymer's specific heat at constant pressure and thermal conductivity, respectively, L_c and $\dot{\theta}$ are the latent heat and rate of crystallization, respectively, $\mathbf{g}$ denotes the gravitational acceleration, and σ denotes the stress tensor. In this paper, ρ, C_p, K and L_c are assumed to be constant.

The deviatoric stress tensor, σ, is assumed to consist of Newtonian (σ_n) and polymeric parts (σ_p), i.e., $\sigma = \sigma_n + \sigma_p$, where the Newtonian contribution may be written as

$$\sigma_n = \mu(T, s)(\nabla v + (\nabla v)^T), \tag{4}$$

where $\mu(T, s)$ is an effective dynamic viscosity that depends on both the temperature and the degree of crystallinity as

$$\mu(T, s) = \mu_T(T)\mu_\theta(\theta), \qquad \mu_T(T) = \mu_0 \exp(E/RT), \qquad \mu_\theta(\theta) = \beta \exp(-(\theta/\theta_\infty)^n), \tag{5}$$

μ_0, E and R are a (constant) dynamic viscosity, the activation energy and the universal gas constant, respectively, θ is the degree of crystallization, i.e., the volumetric fraction of the crystalline phase, θ_∞ is the ultimate degree of crystallization, and β and n are constants that must be determined experimentally. For amorphous polymers, $\theta = 0$ and $\beta = 1$, so that the effective dynamic viscosity only depends on the temperature and increases in an exponential as the temperature is decreased.

The polymeric contribution to the deviatoric stress tensor may be written as

$$\sigma_p = 3ck_BT \left(-\lambda_r \frac{\mathbf{F}(\mathbf{S})}{\phi} + 2\lambda_r ((\nabla \mathbf{v})^T : \mathbf{S}) \left(\mathbf{S} + \frac{1}{3}\mathbf{I} \right) \right), \tag{6}$$

where $\mathbf{S}$ is the molecular orientation tensor, k_B is Boltzmann's constant, $\mathbf{I}$ is the identity or unit tensor, ϕ $(0 \leq \phi \leq 1)$ is a non-dimensional friction coefficient, c is the polymer number density, $\mathbf{F}(\mathbf{S})$ is a function that characterizes the molecular orientation independently of the flow, and λ_r is a relaxation time. In the dumbbell model employed in this study, small values of ϕ correspond to increasing the ratio of the resistance encountered perpendicularly to the dumbbell to that parallel to the axis of the dumbbell, whereas $\phi = 1$ corresponds to an isotropic friction tensor.
The relaxation time that appears in Eq. (6) is associated with the rotation of the dumbbell molecules and may depend on the temperature, degree of crystallization, molecular orientation, and flow. In this paper, it is assumed that λ_r depends only on the temperature through the following Arrhenius expression

$$\lambda_r = \lambda_0 \exp(-E_r/RT), \tag{7}$$

where λ_0 and E_r are constants that denote a characteristic relaxation time and an activation energy, respectively.
As indicated in Eq. (6), the polymeric contribution to the stress tensor depends on the molecular orientation tensor; the latter has been modelled by means of the probability function formulation for the molecular orientation vector $\mathbf{u}$ proposed by Doi and Edwards [27], where $\mathbf{u}$ denotes the molecule's end–to–end vector. By taking moments of the probability density function and modelling the fourth-order moments of the molecular orientation vector in terms of second–order ones, so that a closed system of equations is obtained, one may derive the following transport equation for the molecular orientation tensor

$$\mathbf{v} \cdot \nabla \mathbf{S} - ((\nabla \mathbf{v}) \cdot \mathbf{S} + \mathbf{S} \cdot \nabla \mathbf{v}) = \mathbf{F}(\mathbf{S}) + \mathbf{G}(\mathbf{S}, \nabla \mathbf{v}), \tag{8}$$

where the left–hand side denotes the steady upper Convective Maxwell (UCM) derivative of the tensor $\mathbf{S}$, and

$$\mathbf{F}(\mathbf{S}) = -\frac{\phi}{\lambda_r}\left(\left(1 - \frac{1}{3}N\right)\mathbf{S} - N(\mathbf{S}\cdot\mathbf{S}) + N(\mathbf{S}:\mathbf{S})\left(\mathbf{S} + \frac{1}{3}\mathbf{I}\right)\right), \tag{9}$$

$$\mathbf{G}(\mathbf{S}, \nabla \mathbf{v}) = \frac{1}{3}(\nabla \mathbf{v} + (\nabla \mathbf{v})^T) - 2((\nabla \mathbf{v})^T : \mathbf{S})\left(\mathbf{S} + \frac{1}{3}\mathbf{I}\right), \tag{10}$$

N is a dimensionless measure of the polymer number density c and is proportional to the excluded volume between two rigid rods where each rod represents a polymer molecule, $\mathbf{G}(\mathbf{S}, \nabla \mathbf{v})$ accounts for the interaction between the flow and the molecular orientation, the second term in the left-hand side of Eq. (8) is the rate of molecular orientation induced by straining, the molecular orientation tensor $\mathbf{S} = < \mathbf{u}, \mathbf{u} > -\mathbf{I}/3$ is a traceless tensor, and $< \psi, \psi >$ denotes expected or mean value squared.
For the slender planar films considered in this study, the flow field is mainly elongational and the molecular orientation tensor is diagonal in a first–order approximation in the

slenderness ratio. Since this tensor is traceless, this means that one of its (diagonal) components may be related to the other two in a first–order approximation. For films that are not slender, the six components of the molecular orientation tensor must be retained in the formulation.
The degree of crystallization is governed by Ziabicki's model [26, 28, 29], i.e.,

$$\dot{\theta} = \mathbf{v} \cdot \nabla\theta = k(s)(\theta_\infty - \theta), \tag{11}$$

where $k(s) = k(0)\exp(Bs^2)$ is the crystallization rate and increases exponentially with the molecular orientation order parameter s, B is a positive constant, and $k(0)$ is the amorphous growth rate.
The molecular orientation order parameter that appears in Eq. (11) can be determined from the second invariant of the molecular orientation tensor as [22]

$$s^2 = \frac{3}{2}(\mathbf{S} : \mathbf{S}). \tag{12}$$

s affects the dynamic viscosity of the Newtonian contribution to the deviatoric stress tensor through Eq. (5). This means that the molecular orientation order parameter affects directly the crystallization rate through Eq. (11) and indirectly the flow field through the Newtonian stress tensor; the flow field, in turn, affects directly the molecular orientation tensor and the temperature field.
Equations (1)–(3), (8), (11) and (12) are nonlinearly coupled through the dependence of the Newtonian dynamic viscosity on both the temperature and the degree of crystallization, the dependence of the polymeric stress tensor on the temperature and molecular orientation, and the dependence of the degree of crystallization on the molecular orientation and velocity field.
Equations (1), (8) and (11) are first-order partial differential equations. Equation (1) is a constraint that may be used to determine the pressure field from the divergence of the linear momentum equations that results in an elliptic equation for the pressure. Equation (11) is a linear first–order partial differential equation for θ that may be written as a system of three first–order ordinary differential equations by introducing a time–like variable, or as a system of two first–order of differential equations. A similar comment applies to the six components of the molecular orientation tensor the evolution of which is governed by Eq. (8).
For the three-layer films considered in this study, boundary conditions for the molecular orientation and degree of crystallization were specified at the die's exit for both the core and the cladding; symmetry conditions were imposed at $y = 0$ for these two variables in the core, while the normal derivative of the degree of crystallization and the molecular orientation was set to zero at the core–cladding interface when determining these variables in the cladding. The velocity and temperature fields were specified at the die's exit and were subject to symmetry conditions at the film's axis, and kinematic, dynamic and thermal boundary conditions at both the core–cladding interface and the film's or cladding's

outer surface. For example, at the core–cladding interface, the velocity components, the temperature, the shear stress and the heat flux normal to that interface are continuous, $v(x, h(x)/2) = u(x, h(x)/2)h'(x)/2$ where $h'(x) = dh(x)/dx$, while the difference between the normal stresses on both sides of the interface is balanced by surface tension. Since for slender films, the slenderness ratio and the curvature are small, surface tension may be neglected, although it could be important for small draw ratios and/or non–slender films. Similar conditions to the ones described above for the core–cladding interface were imposed at the film's outer surface and this required to solve for the velocity and temperature fields of the gases that surround the film. These gases were considered ideal and their dynamics was assumed to be represented by a boundary layer approximation which is justified when the (gas) Reynolds number is large enough and, therefore, cooling gases are blown over the film's outer surface at high speeds. Under these conditions, the pressure on the gases does not depend on y, the gas transverse momentum equation can be disregarded and the gas axial momentum and energy equations are governed by parabolic equations.

At the chill roll, the value of u was specified, i.e., the film's draw longitudinal velocity was assumed to be uniform, while the gradients of v and T normal to that boundary were set to zero. These conditions are adequate when the film solidifies before it is collected at the chill roll; when this does not occur, the longitudinal velocity component may not be uniform at the chill roll location and a solidified shell may form at the film's outer surface. In such a case, the normal derivative of the longitudinal velocity at the chill roll was set to zero only for the molten polymer, and mass conservation was used to determine the longitudinal velocity of the solidified polymer at that location.

The gas pressure, temperature and velocity fields far away from the film's outer surface were specified at either the die's exit or the take–up roll depending on whether the cooling gases were blown along the film from the die's exit towards the take–up roll or in the opposite direction, respectively.

Calculations have also been performed without solving for the dynamics and thermal fields of the gases that surround the film. In such a case, the shear stress at the film's outer surface was set to zero on account of the fact that the dynamic viscosity of gases is usually much smaller than that of the film's molten polymer, the pressure of the gases that surround the film was assumed constant, the deviatoric stress in the gas was neglected, and the heat flux at the film's outer surface was determined from the following heat transfer correlations for laminar flow [30, 31]

$$h_t = h_f + h_n + h_r, \quad h_f = 0.66\frac{K_a}{x}Re^{1/2}Pr^{1/3}, \quad h_n = 0.56\frac{K_a}{x}Ra^{1/4}, \tag{13}$$

where h_i with $i = f, n, r$ and t, is the film heat transfer coefficient, $Re = xu_t/\nu_a$, $Pr = C_a\mu_a/k_a$, $u_t = u - u_a$, $Ra = gx^3(T(x, h(x)/2 + H(x)) - T_a)/\nu_a^2 T_a$, Re, Pr and Ra are the Reynolds, Prandtl and Rayleigh numbers, respectively, ν denotes the kinematic viscosity, the subscripts a, n, f and r refer to the gas surrounding the film, natural and

forced convection, and radiation, respectively, u_a and T_a are the velocity component of the cooling gases along the film's outer surface and the temperature far from the film, $h_r = \epsilon\sigma(T^4 - T_a^4)/(T - T_a)$, σ is the Stefan–Boltzmann constant and ϵ is the emissivity of the polymer film which depends on the film thickness.
The radiant transmissivity of polymer films varies quite dramatically with the wavelength. An average value of ϵ may be obtained from the transmissivity as [32]

$$\epsilon = \frac{1}{\lambda_2 - \lambda_1} \int_{\lambda_1}^{\lambda_2} (1 - \tau(\lambda, e(x)))d\lambda, \tag{14}$$

where λ and τ denote the wavelength and transmissivity, respectively, and $e(x)$ denotes the film's thickness. For 25 and 250 μm films of propylene, Lamberti et al. [8, 9] found that the average emissivity was 0.167 and 0.467, respectively, and experimental data [11] indicate that the dependence of the emissivity of films on their thickness may be written as $\epsilon = 1 - \exp(-be(x))$ where b is a function of the temperature. This expression satisfies the condition that $\epsilon = 0$ for $e(x) = 0$ and $\epsilon = 1$ as $e(x) \to \infty$, and is usually a good approximation. Furthermore, for isopropylene (iPP), $b = 2662$ m^{-1} which is the value used here.

3 NUMERICAL METHODS

Two different numerical methods have been used to solve Eqs. (1)-(3), (8), (11) and (12). The first method is based on transforming the curvilinear geometries of the core and cladding into unit squares, whereas the second one employs a transformation from the physical coordinates to streamline coordinates. In the next two subsections, these techniques are described.

3.1 Transformation of coordinates

As stated in Section 2, the core and cladding correspond to $0 \le y \le h(x)/2$ and $h(x)/2 \le y \le h(x)/2 + H(x)$, respectively. The curvilinear geometries of both the core and the cladding can be transformed into unit squares by means of the transformations $(x, y) \to (\xi_c, \eta_c)$ and $(x, y) \to (\xi_{cl}, \eta_{cl})$, respectively, where $\xi_c = x/L$, $\xi_{cl} = x/L$, $\eta_c = 2y/h(x)$ and $\eta_{cl} = (y - h(x)/2)/H(x)$, the subscripts c and cl denote the core and cladding, respectively, and L denotes the film's length, i.e., the distance between the die's exit and the chill roll. With these two transformations, the die's exit and the chill roll locations are mapped to $\xi_c = \xi_{cl} = 0$ and 1, respectively; the symmetry axis, the core–cladding interface, and the film's outer surface are mapped to $\eta_c = 0$, $\eta_c = 1$ and $\eta_{cl} = 0$, and $\eta_{cl} = 1$, respectively.
By means of these two mappings, Eq. (1) becomes

$$(uA)_\xi + (v_e)_\eta = 0, \tag{15}$$

where $v_e = v - u(B' + \eta A')$ with $A = h(x)/2$ and $B = 0$ for the core, and $A = H(x)$ and $B = h(x)/2$ for the cladding, represents a relative velocity, while the advection operator

in Eqs. (2)-(3), (8) and (11) may be written as

$$u\phi_x + v\phi_y = \frac{1}{A}((Au\phi)_\xi + (v_e\phi)_\eta), \tag{16}$$

and, therefore, the above equations can be written in strong conservation–law form for u, v, $\mathbf{S}$, θ and T. The resulting equations were then discretized by means of a finite–volume method in a staggered grid where the scalar variables were evaluated at the grid points, while the velocity components were determined at the cell boundaries.

At the low Reynolds numbers that characterize film casting processes, the convection terms in the linear momentum equations were discretized by means of second–order accurate finite difference formulae. Since the equations for the molecular orientation tensor and the degree of crystallization are of the advective type, the fluxes at the cell boundaries were evaluated by means of first–order accurate upwind differences; the same type of differences was employed to evaluate the convective terms of the energy equation at high Péclet numbers, while these terms were evaluated by means of second–order central differences at the cell boundaries at low thermal Péclet numbers.

When imposing the continuity of the shear stress conditions at the core–cladding interface and at the film's outer surface when the gas boundary layer over the film was calculated, the velocity gradients at these interfaces were determined by means of first–order, one–side differences; a similar discretization was employed when determining the temperature and velocity gradients at the interfaces between the core and the cladding and between the cladding and the gases that surround the film, although calculations were also performed by using second–order accurate three–point discretizations of the normal derivatives of these variables at the interfaces. The derivatives of $h(x)$ and $H(x)$ that appear in the kinematic boundary conditions at the core–cladding interface and at the film's outer surface were evaluated by means of first–order accurate formulae.

The pressure field was determined from the Poisson equation that results from taking the divergence of the linear momentum equations [33]. Note that the partial derivative of the pressure with respect to x can be written as $p_x = ((pA)_\xi - (pC)_\eta)/A$ where $C = B' + \eta A'$ and, therefore, the longitudinal momentum equation is affected by the pressure gradient components in the two transformed coordinates; this does not occur in the transverse momentum equation.

Two different strategies were followed to obtain the solution of the discretized form of Eqs. (1)-(3), (8) and (11). In the first strategy, Eqs. (1)–(3) were solved in an iterative fashion with assumed values of the molecular orientation tensor and degree of crystallization until a user's specified criterion was satisfied. Once convergence of these equations was achieved, Eqs. (8) and (11) were solved iteratively until they were satisfied to a prescribed tolerance. With the molecular orientation tensor and degree of crystallization thus obtained, Eqs. (1)–(3) were then solved again and this iterative two–cycle process was repeated until the user's specified error tolerances on the residuals of the linear momentum, energy, molecular orientation tensor, degree of crystallization and continuity equations were satisfied. Due

to the nonlinear coupling amongst the continuity, linear momentum and energy equations and the strong dependence of the dynamic viscosity on temperature, under–relaxation was required; typical under–relaxation factors for the longitudinal and transverse momentum equations and the energy equations are 0.37, 0.42 and 0.54, respectively, whereas the under–relaxation factor for the pressure was found to be about 0.74.
Although the iterative two–cycle procedure described in the previous paragraph was found to converge in most of the cases considered in this study where the initial velocity, pressure and temperature fields were assumed to be those obtained numerically from a one–dimensional model that was deduced from Eqs. (1)-(3), (8) and (11) by means of asymptotic methods for small slenderness ratios and small Reynolds and Biot numbers [25], its convergence was found to be slow when there is a strong contraction of the film at the die's exit where forced convection and radiation heat exchanges are very important; this is usually the case at high drawing ratios or for very slender fibers. In these cases, it was found that an iterative procedure that consists in solving the discretized forms of Eqs. (1)-(3), (8) and (11) simultaneously requires fewer iterations for convergence provided that the initial guess is sufficiently close to the solution and the under–relaxation factors are properly selected.
When the dynamics of the gases that surround the film were considered, a similar transformation of coordinates to that employed in the core and cladding was employed; in this case, the gas flow was assumed to be uniform at a transversal location about three times the boundary layer thickness. As stated above, the use of a boundary layer approximation for the gases that surround the film is a reasonable approximation provided that the gas Reynolds number is sufficiently large and this requires large longitudinal gas velocities and/or long films; such conditions were not met in some simulations at low drawing ratios. When this occurred, the heat transfer correlations described in the previous section were used and, therefore, the dynamics of the gases surrounding the film was not considered.

3.2 Streamline coordinates

Since the molten polymers considered in this study are assumed to be incompressible, one may use the transformation $(x, y) \rightarrow (\xi, \psi)$ where $\xi = x$ and $\psi(x, y)$ is the stream function, i.e., $u = \psi_y/L$ and $v = -\psi_x/L$, so that Eq. (1) is no longer required, for it is satisfied by the stream function. Furthermore, by nondimensionalizing the stream function with respect to the sum of the volumetric flow rates of the core and cladding and setting $\psi = 0$ at the film's axis, the core–cladding interface and the film's outer surface correspond to $\psi_c = \dot{V}_c/\dot{V}$ and $\psi_{cl} = 1$, respectively, where $\dot{V}_c$ and $\dot{V}$ denote the core's volumetric flow rate and the total volumetric flow rate, respectively, i.e., $\dot{V} = \dot{V}_c + \dot{V}_{cl}$.
Upon introducing the above transformation into Eqs. (2)-(3), (8) and (11), the advection operator becomes

$$u\phi_x + v\phi_z = u\phi_\xi, \tag{17}$$

and, therefore, Eqs. (2) and (3) become parabolic equations, and their discretization is

not subject to the magnitude of the cell Reynolds or thermal Péclet number as the one described in the previous section; these equations may be used to determine u, v and T, whereas the pressure may be obtained from the Poisson equation that results from taking the divergence of the linear momentum equation. In addition, the kinematic boundary conditions correspond to constant values of the stream function and, therefore, the film's outer surface can be obtained from the total differentiation of $\psi(x, h(x)/2+H(x)) = 1$ with respect to x which yields $v(x, h(x)/2+H(x)) = u(x, h(x)/2+H(x))(h'(x)/2+H'(x))$ and may be used to determine $H(x)$; a similar expression holds at the core–cladding interface. A disadvantage of the stream function formulation presented here is that the discretization is performed in the (ξ, ψ) coordinates and the transverse coordinate must be obtained from $y = \int_0^{\psi} d\phi/u(\xi, \phi)$ and, therefore, varies with $\xi = x/L$.
A finite–volume method similar to the one described in the previous section was used to determine u, v, p, T, $\mathbf{S}$ and θ as functions of (ξ, ψ). u was then used to determine the value of y as discussed in the previous paragraph, except that the discretized equations were solved in only one iterative cycle starting with the numerical solution of the one–dimensional model described in the previous section. Streamline coordinates were only used when heat transfer correlations at the film's outer surface were employed to account for the convection and radiation heat exchanges between the film and its surroundings. It must be noted that streamlines coordinates can also be used for compressible polymers; in that case, the stream function corresponds to a mass flow rate and is constant at both the core–cladding interface and the film's outer surface, but the kinematic condition at these interfaces are more complex than that for constant density polymers.

4 PRESENTATION OF RESULTS

Calculations were first performed for compound and hollow–compound fibers and three–layer planar films with the two numerical formulations described in the previous section. It was observed that the differences between the results obtained with these formulations were less than 1.1 % for the nondimensional longitudinal velocity component and temperature, molecular orientation parameter and degree of crystallization, and the largest differences were found near the die's exit for draw ratios of 20 when the same number of grid points were employed in both formulations; the draw ratio is the film's thickness at the die's exit divided by the film's thickness at the chill roll.
It must be noted that the grid spacing was not uniform in the longitudinal and transverse directions; in fact, calculations were first performed in equally–spaced grids in order to determine the locations of the largest gradients and the grid was then refined near these locations subject to the restriction that the ratio of the sizes of adjacent cells had to be between 0.71 and 1.41. Grid points were concentrated near the core–cladding interface, near the film's outer surface and near the die's exit where the largest gradients are expected.
Figure 2 shows the distributions of the molecular orientation parameter (left) and the degree of crystallization (right) for a three–layer film; the dashed line in this figure denotes the core–cladding interface. This figure indicates that almost full molecular orientation

is achieved near the die's exit due to the strong contraction that the film experiences upon exiting the die, thus indicating that, for the conditions considered in this figure, the molecular orientation is mainly driven by the strain rate in accord with Eq. (8). On the other hand, for the small values of the amorphous growth rate, $k(0)$, considered for the cladding, very little crystallization is observed in the film's outer surface, whereas the crystallinity of the core increases along the film but it never reaches its ultimate value θ_∞ and is not uniform at the chill roll location, although its transverse variation is small at that location.

As stated in Section 2, the models for the molecular orientation tensor and the degree of crystallization considered in this study are governed by first–order partial differential equations, and, therefore, the molecular orientation and crystallization of the core depend on the boundary conditions at the film's symmetry axis and at the die's exit, as well as the flow and temperature fields in the three–layer film. As a consequence the molecular orientation and the degree of crystallization may not be continuous at the core–cladding interface even though the velocity and temperature fields are continuous there. At that interface, one would expect that there is some entanglement between the polymer molecules of the core and cladding that may result in a transition layer where the molecular orientation is adjusted from that of the core to that of the cladding. Since such a transition layer has not been modelled in the formulation presented here, one may observe that molecular orientation parameter may be discontinuous at the core–cladding interface. A similar comment applies to the degree of crystallization, as illustrated in Figure 2 (right).

The large contraction that the film experiences upon exiting the die's exit is shown in Figure 3 which illustrates both the three–layer film geometry and the nondimensional temperature distribution for cooling gases blown from the location of the chill roll towards the die's exit; the nondimensional temperature has been defined as $(T-T_0)/(T_a-T_0)$ where T_0 denotes the cross–section averaged temperature at the die's exit. For the conditions considered in Figure 3, the relative velocity between the film and the surrounding gases is larger than when cooling gases are blown from the location of the die's exit towards the chill roll and results in an increase of the heat transfer rate and a large temperature drop near the die's exit where forced convection and radiation are dominant.

Figure 3 also indicates that the nondimensional cross–section averaged temperature at the chill roll is about 40 % of that at the die's exit and that the film's thickness is almost constant for $\hat{x} \gtrsim 0.5$. Since the dynamic viscosity of the Newtonian rheology employed in this paper increases exponentially as the film's temperature decreases, it may be stated that the solidification observed in Figure 3 is associated with the increase of the dynamic viscosity with a very small contribution due to the crystallization which was found to be rather small in the cladding as illustrated in Figure 2.

The results presented in Figures 2 and 3 indicate that the flow–induced crystallization is much less important than thermal crystallization. In fact, as the temperature decreases and the dynamic viscosity increases, the longitudinal velocity component tends to a constant value, the elongation rate decreases, and so does the molecular orientation; this

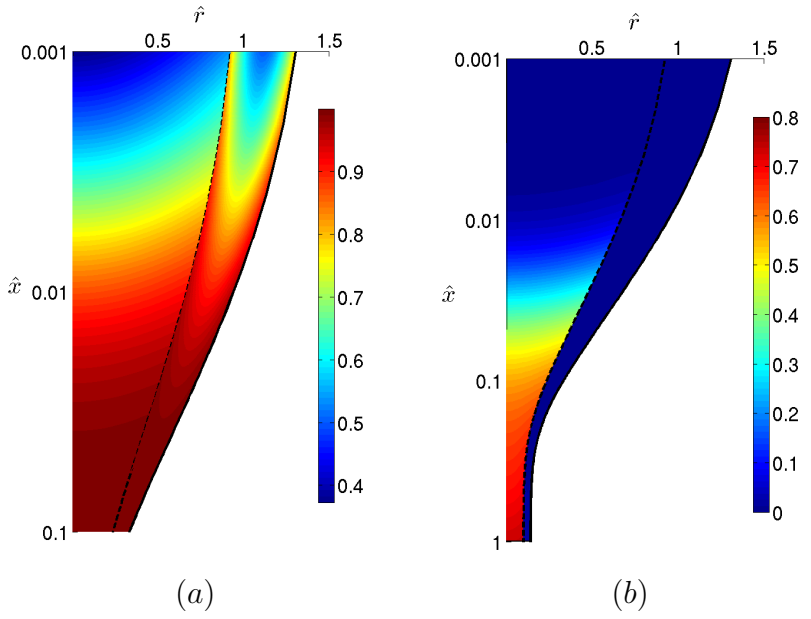

Figure 2: Distributions of the molecular orientation order parameter (left) and degree of crystallization (right) in nondimensional coordinates. ($\hat{x} = x/L$ and $\hat{r} = y/H_0$ where H_0 is a characteristic film thickness at the die's exit.)

means that the crystallization rate which depends on the current values of the molecular orientation and crystallinity, decreases as the temperature decreases. Furthermore, for the conditions considered in this study, the contribution of the latent heat of crystallization that results in a local increase of the temperature is less important than that associated with flow convection and heat transfer losses. Only at draw ratios higher than about 200 and small heat exchanges between the film and the surroundings, latent heat effects and flow–induced crystallization were found to be important.

For the conditions considered in Figures 2 and 3, the film's cross–section averaged longitudinal velocity component exhibits a sigmoid shape characterized by a large increase near the die's exit, the presence of an inflection point at $\hat{x} \approx 0.25$, a change of convexity for larger values of $\hat{x}$ and a constant value equal to the chill roll speed for $\hat{x} \gtrsim 0.45$. However, for smaller draw ratios and activation energies of the dynamic viscosity than the ones considered in Figures 2 and 3, the average longitudinal velocity component was found to be monotonically increasing from the die's exit to the chill roll and did not exhibit an inflection point, as illustrated in Figure 4.

For small draw ratios and activation energies of the dynamic viscosity, the degree of molecular orientation was found to increase from the die's exit but full molecular orientation might not be reached at the chill roll. Since the degree of crystallization is mainly controlled by the velocity field and the molecular orientation, the crystallization was found to decrease as the draw ratio and the heat exchanges were decreased. Moreover, in some

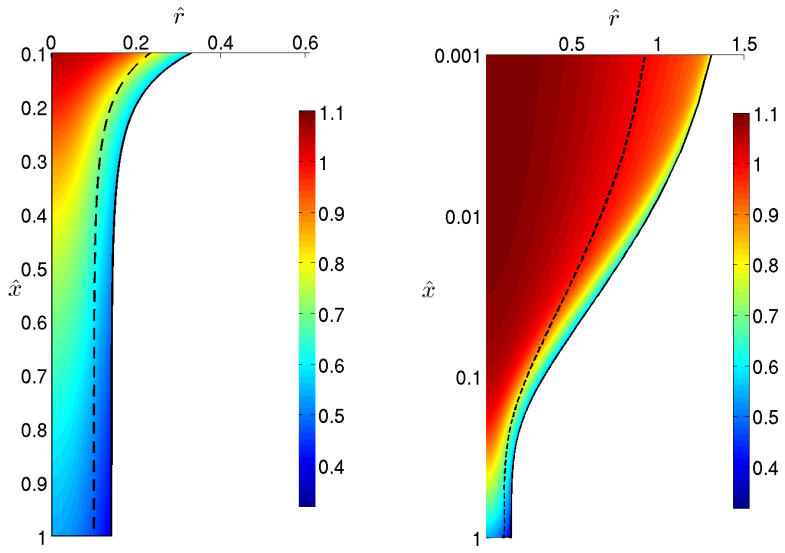

(a) (b)

Figure 3: Nondimensional temperature distribution in nondimensional coordinates. ($\hat{x} = x/L$ and $\hat{r} = y/H_0$ where H_0 is a characteristic film thickness at the die's exit.)

cases, it was also observed that the molecular orientation increases from the die's exit until a longitudinal location where it reaches a relative maximum and then decreases slowly along the drawing direction. This is clearly unrealistic and was found to be caused by the sink term that appears in the transport equation for the molecular orientation tensor.
For cooling gases blown from the chill roll towards the die, the film's cross–section averaged temperature was found to decrease at a faster rate than when the cooling gases were blown in the opposite direction due to the increase in forced convection heat exchanges; this increase in heat transfer results in a larger contraction of the film at the die's exit, larger values of the dynamic viscosities of the core and cladding and a steeper increase of the degree of molecular orientation than in the absence of forced convection; however, the degree of crystallization reached smaller values at the chill roll.
For the two smaller cooling rates shown in Figure 4, the cross–section averaged longitudinal velocity component exhibits a steep gradient at the chill roll location where the film is collected and the slope of the film's thickness is not constant there, thus indicating that the film has not solidified. This can also be observed in the small temperature drop along the film and the small increase in dynamic viscosity. On the other hand, the molecular orientation order parameter increases along the film and tends to its asymptotic value of unity, i.e., full molecular orientation, at a rate that increases as the cooling rate is increased. Since, as stated above, the degree of crystallization in the formulation presented here is controlled by the molecular orientation, the crystallinity increases along the fiber towards its ultimate value $\theta_\infty = 0.8$ and its rate increases as the molecular orientation

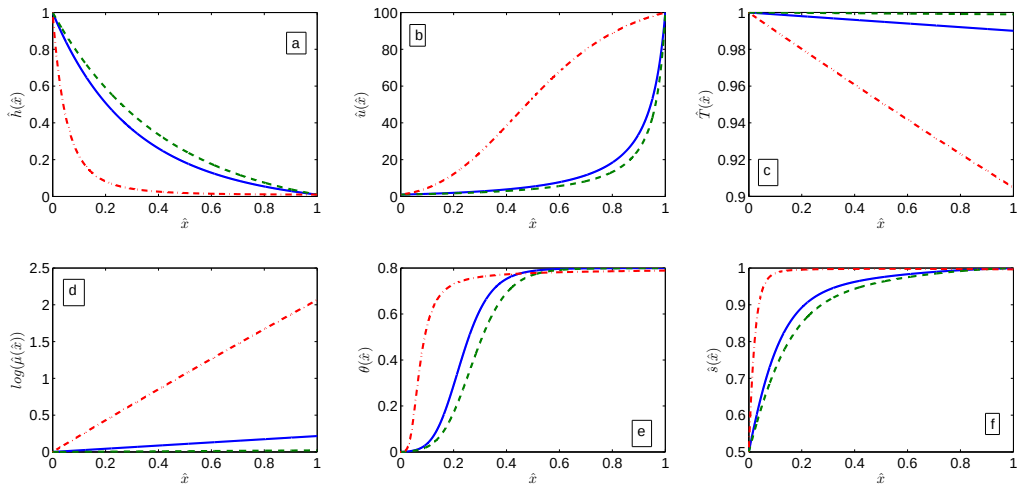

Figure 4: Nondimensional film thickness (a) and cross–section averaged axial velocity component (b), temperature (c), dynamic viscosity of the Newtonian rheology (d), degree of crystallization (e) and molecular orientation parameter (f) for three cooling rates. ($\hat{x} = x/L$ and $\hat{r} = y/H_0$ where H_0 is a characteristic film thickness at the die's exit.)

increases.

Figure 4 also shows that the rate of molecular orientation increases as the straining rate increases; for high cooling rates, the film experiences a large contraction near the die's exit due to forced convection and radiation heat exchanges there that result in a high straining rate there. For low cooling rates, however, the longitudinal velocity component increase rapidly near the chill roll and the straining rate is higher there.

In the absence of forced convection, it was found that the radiative heat exchange between the three-layer film and the surroundings was about 37%; however, for cooling gases blown from the chill roll towards the die's exit, the forced convection and radiation heat exchanges at the film's outer surface were approximately 53 and 32 percent, respectively, and the contribution of natural and forced convection and radiation was found to depend very strongly on the draw ratio, the magnitude and direction of the velocity of the cooling gases, the ambient temperature and the parameters that characterize the dynamic viscosity law, the relaxation time and the crystallization rate. For example, for a draw ratio of twenty, it was found that forced and natural convection heat exchanges at the film's outer surface contributed approximately 41 and 33 percent, respectively, to the total heat exchange, while an increase in the activation energy that characterizes the dynamic viscosity might not yield a solidified film.

A comparison between the truly two–dimensional model presented here and a hybrid model that employs the one-dimensional equation for the longitudinal velocity derived

from an asymptotic analysis for slender films at low Reynolds and Biot numbers indicates that the predictions of these two models are in qualitative accord even for small draw ratios, but large differences are observed near the film's outer surface where the truly two–dimensional model predicts a larger longitudinal velocity component than the hybrid one and near the die's exit where the hybrid model predicts a larger contraction than the truly two–dimensional one. These differences may be attributed to the fact that the hybrid model uses a one–dimensional momentum equation which is only valid for slender fibers at low Reynolds numbers, and decrease as the draw ratio is increased or the slenderness ratio is decreased. They can also be attributed to the fact that the one–dimensional momentum equation of the hybrid model uses cross-section averaged values of the temperature, dynamic viscosity, molecular orientation and degree of crystallization. However, the two–dimensional hybrid model is computationally more efficient, for the core–cladding interface and the film's outer surface are governed by one–dimensional equations which correspond to the conservation of mass in the core and cladding, and the dynamic boundary conditions at the core–cladding and film's outer interface are incorporated in the one–dimensional linear momentum equation.

5 CONCLUSIONS

A formulation for the study of planar film casting of incompressible, liquid–semicrystalline polymers that accounts for the molecular orientation and crystallization has been presented. The formulation includes transport equations for the molecular orientation and the degree of crystallization, uses a homogeneous two–phase flow approximation, and accounts for Newtonian and polymeric contributions to the deviatoric stress tensor through a dynamic viscosity that depends on the temperature and molecular orientation, while the degree of crystallization is controlled by the flow field and the molecular orientation. The formulation is applicable to multi–layer films, and compound and hollow–compound polymeric fibers.

Two methods have been proposed to solve the governing equations. The first employs a transformation that maps the physical three–layer film into two unit squares and the strong conservation–law of the equations in the transformed coordinates where a finite–volume discretization has been carried out. Two iterative procedures have been used to solve the discretized equations. The first iterative method uses a two–cycle approach whereby the continuity, linear momentum and energy equations are solved independently of those for the molecular orientation tensor and the degree of crystallization, and the latter are then solved using the previously known values of the velocity and temperature fields. In the second iterative procedure, all the discretized equations are solved in block form, using under–relaxation.

The second transformation method employs a transformation of coordinates based on the stream function and results in parabolic equations which were discretized by means of a finite–volume method and solved in a block form. It has been found that the two formulation yield very close results for the three–layer films considered in this study, as

well for compound and hollow–compound fibers.
It has been shown that, due to the strong contraction that the film experiences near the die's exit, full molecular orientation is reached close to the die, but the ultimate degree of crystallization may not be reached at the chill roll location. It was also found that, depending on the operating conditions, the transverse distribution of crystallinity at the chill roll location may not uniform; such a non–uniformity has a strong effect on the mechanical, physical, chemical and optical properties of the three–layer film.

ACKNOWLEDGEMENTS

The author was supported by Project FIS2012-38430 from the Ministerio de Economía y Competitividad of Spain.

REFERENCES

[1] J. F. Agassant, Y. Demay, C. Sollogoub and D. Silagy, Cast film extrusion, *Int. Polym. Process.*, Vol. **20**, pp. 136–148, (2005).

[2] V. R. Iyengar and A. Co, Film casting of a modified Giesekus fluid: a steady-state analysis, *Int. J. Non-Newtonian Fluid Mech.*, Vol. **48**, pp. 1–20, (1993)

[3] P. Carlone, G. S. Palazzo and R. Pasquino, Modelling of film casting manufacturing process longitudinal and transverse stretching, *Math. Comput. Model.*, Vol. **42**, pp. 1325–1338, (2005).

[4] T. Dobroth and L. Erwin, Causes of edge beads in cast films, *Polym. Eng. Sci.*, **26**, pp. 462–467, (2004).

[5] B. Scheid, S. Quiligotti, B. Tran and H. A. Stone, Lateral shaping and stability of a stretching viscous sheet, *Eur. Phys. J. B*, Vol. **68**, pp. 487–494, (2009).

[6] G. Barot and I. J. Rao, Modeling the film casting process using a continuum model for crystallization in polymers, Int. J. Non-Linear Mech., Vol. **40**, pp. 939–955, (2005).

[7] M. Beaulne and E. Mitsoulis, Numerical simulation of the film casting process, *Int. Polymer Process.*, Vol. **14**, pp. 261–275, (1999).

[8] G. Lamberti, G. Titomanlio and V. Brucato, Measurement and modelling of the film casting process 1. Width distribution along draw direction, *Chem. Eng. Sci.*, Vol. **56**, pp. 5749–5761, (2001).

[9] G. Lamberti, G. Titomanlio and V. Brucato, Measurement and modelling of the film casting process 2. Temperature distribution along draw direction, *Chem. Eng. Sci.*, Vol. **56**, pp. 5749–5761, (2001).

[10] K. Nakamura, T. Watanabe, K. Katayama and T. Amano, Some aspects of non-isothermal crystallization of polymers, *J. Appl. Polymer Sci.*, Vol. **16**, pp. 1077–1091, (1972).

[11] P. Barq, J. M. Haudin and J. F. Agassant, Isothermal and anisothermal models for cast film extrusion: A viscoelastic approach, *Int. Polymer Process.*, Vol. **7**, pp. 334–349, (1992).

[12] S. Shiromoto, The mechanism of neck-in phenomenon in film casting process, *Int. Polymer Process.*, Vol. **29**, pp. 197–206, (2014).

[13] O. Zavinska, J. Claracq and S. van Eijndhoven, Non-isothermal film casting: Determination of raw resonance, *Int. J. Non-Newtonian Fluid Mech.*, Vol. **151**, pp. 21–29, (2008).

[14] D. Silagy, Y. Demay, and J. F. Agassant, Numerical simulation of the film casting process, *Int. J. Numer. Meth. Fluids*, Vol. **30**, pp. 1–18, (1999).

[15] N. R. Anturkar and A. Co, Draw resonance in film casting of viscoelastic fluids: A linear stability analysis, *Int. J. Non-Newtonian Fluid Mech.*, Vol. **28**, pp. 287–307, (1988).

[16] K. Christodoulou, S. G. Hatzikiriakos and D. Vlassopoulos, Stability analysis of film casting of PET resins using a multimode Phan-Thien-Tanner constitutive equation, *J. Plastic Film Sheet.*, Vol. **16**, pp. 312–332, (2000).

[17] K. Sakaki, R. Katsumoto, T. Kajiwara and K. Funtasu, Three-dimensional flow simulation of a film-casting process, *Polym. Eng. Sci.*, Vol. **36**, pp. 1821–1831, (1996).

[18] J. M. Kim, J. S. Lee, D. M. Shin, H. W. Jung and J. C. Hyun, Transient solutions of the dynamics of film casting process using a 2-D viscoelastic model, *Int. J. Non-Newtonian Fluid Mech.*, Vol. **132**, pp. 53–60, (2005).

[19] D. M. Shin, J. S. Lee, J. M. Kim, H. W. Jung and J. C. Hyun, Transient and steady-state solutions of 2D viscoelastic nonisothermal simulation model of film casting process via finite element method, *Int. J. Non-Newtonian Fluid Mech.*, Vol. **51**, pp. 393–407, (2007).

[20] C. Sollogoub, Y. Demay and J. F. Agassant, Non-isothermal viscoelastic numerical model of cast-film process, *Int. J. Non-Newtonian Fluid Mech.*, Vol. **138**, pp. 76–86, (2006).

[21] N. Satoh, H. Tomiyama and T. Kajiwara, Viscoelastic simulation of film casting process for a polymer melt, *Polym. Eng. Sci.*, Vol. **41**, pp. 1564–1579, (2001).

[22] J. I. Ramos, *Heat transfer processes in film casting of compressible polymers*, Paper IHTC15–9814, Proceedings of the 15th International Heat Transfer Conference, IHTC-15, Begell House, Inc., New York, (2014).

[23] F. J. Blanco-Rodríguez and J. I. Ramos, Melt spinning of semi-crystalline compound fibers, *Polymer*, Vol. **52**, pp. 5573–5586, (2011).

[24] F. J. Blanco-Rodríguez and J. I. Ramos, A simplified two-dimensional model of the melt spinning of semi-crystalline hollow compound fibers, *Int. J. Thermal Sci.*, Vol. **58**, pp. 102–112, (2012).

[25] J. I. Ramos, Modelling of liquid crystalline compound fibers, *Polymer*, Vol. **46**, No. 26, pp. 12612–12625, (2005).

[26] A. Ziabicki, A. Jarecki and A. Wasiak, Dynamic modelling of melt spinning, *Comput. Theor. Polym. Sci.*, Vol. **8**, pp.143–157, (1988).

[27] M. Doi and S. F. Edwards, *The Theory of Polymer Dynamics*, second edition, Oxford University Press, Oxford, UK, (1988).

[28] A. Ziabicki. *Fundamentals of Fibre Formation*, John Wiley & Sons, New York, (1976).

[29] A. Ziabicki and H. Kawai, *High Speed Fiber Spinning*, John Wiley & Sons, New York, (1985).

[30] J. R. Backhurst, J. H. Harker, J. M. Coulson, J. F. Richardson and R. P. Chhabra, *Fluid Flow, Heat Transfer and Mass Transfer*, Chemical Engineering Series, Vol. 1, sixth revised edition, Butterworth-Heinemann Ltd., New York, (1981).

[31] S. W. Churchill and H. H. S. Chu, Correlating equations for laminar and turbulent free convection from a vertical plate, *Int. J. Heat Mass Transfer*, Vol. **18**, pp. 1323–1329, (1975).

[32] R. Siegel and J. R. Howell, *Thermal Radiation Heat Transfer*, second edition, Hemisphere Publishing Co., New York, (1981).

[33] S. V. Patankar, *Numerical Heat Transfer and Fluid Flow*, second edition, Hemisphere Publishing Co., New York, (1980).